atmosphere

MDPI

Article

Kinetics of the Reactions of Ozone with Halogen Atoms in the Stratosphere

S. Vijayakumar [1,*], Duminda S. Ranasinghe [2] and David M. Wilmouth [1]

[1] Harvard John A. Paulson School of Engineering and Applied Sciences and Department of Chemistry and Chemical Biology, Harvard University, Cambridge, MA 02138, USA; wilmouth@huarp.harvard.edu
[2] Department of Chemical Engineering, Massachusetts Institute of Technology, Cambridge, MA 02139, USA; duminda@mit.edu
* Correspondence: vijay@huarp.harvard.edu

Abstract: It is well established that reaction cycles involving inorganic halogens contribute to the depletion of ozone in the atmosphere. Here, the kinetics of O_3 with halogen atoms (Cl, Br, and I) were investigated between 180 and 400 K, expanding the temperature range relative to prior studies. Canonical variational transition state theory including small curvature tunneling correction (CVT/SCT) were considered, following the construction of the potential energy surfaces. MRCI + Q/aug-ano-pVTZ//MP2/aug-cc-pV(T + d)Z and MRCI + Q/aug-ano-RCC-VTZP//MP2/aug-cc-pV(T + d)Z levels of theory were used to calculate the kinetic parameters. Calculated rate coefficients were used to fit the Arrhenius equations, which are obtained to be $k_1 = (3.48 \pm 0.4) \times 10^{-11} \exp[(-301 \pm 64)/T]$ cm^3 molecule^{-1} s^{-1}, $k_2 = (3.54 \pm 0.2) \times 10^{-11} \exp[(-990 \pm 35)/T]$ cm^3 molecule^{-1} s^{-1} and $k_3 = (1.47 \pm 0.1) \times 10^{-11} \exp[(-720 \pm 42)/T]$ cm^3 molecule^{-1} s^{-1} for the reactions of O_3 with Cl, Br, and I atoms, respectively. The obtained rate coefficients for the reactions of O_3 with halogen atoms using CVT/SCT are compared to the latest recommended rate coefficients by the NASA/JPL and IUPAC evaluations. The reactivity trends and pathways of these reactions are discussed.

Keywords: gas phase kinetics; halogens; ozone; atmosphere; reaction mechanism

Citation: Vijayakumar, S.; Ranasinghe, D.S.; Wilmouth, D.M. Kinetics of the Reactions of Ozone with Halogen Atoms in the Stratosphere. *Atmosphere* **2021**, *12*, 1053. https://doi.org/10.3390/atmos12081053

Academic Editor: Luís Pedro Viegas

Received: 12 July 2021
Accepted: 11 August 2021
Published: 17 August 2021

1. Introduction

The importance of halogens (X = Cl, Br, and I) as catalysts in the destruction of ozone in the atmosphere is well recognized [1]. Halogen source gases are emitted at the surface both naturally and from human activities, and eventually can be photolyzed by sunlight or react chemically to convert their halogen content into inorganic forms. Ozone destruction takes place through a number of different chemical cycles in which halogen atoms are the key reactant in the ozone loss step.

ClO radicals are major contributors to stratospheric ozone loss in the Arctic and Antarctic poles [1,2]. During polar winter and spring, heterogeneous processes convert relatively inert chlorine reservoir species ($ClONO_2$ and HCl) into active, photolabile forms (Cl_2 and HOCl). These photolabile species are rapidly photolyzed in sunlight to produce Cl, which reacts with O_3 to form ClO. Subsequent reaction of ClO with another ClO molecule at cold temperatures to form ClOOCl initiates a catalytic reaction cycle [3,4], which repeatedly forms Cl in sunlight and subsequently destroys O_3 via the Cl + O_3 reaction. This is one of many catalytic ozone-loss cycles at work in the stratosphere, in which a single Cl atom can destroy numerous O_3 molecules [1].

BrO radicals are formed in the atmospheric breakdown of bromine-containing compounds and are similarly involved in ozone destruction occurring in the polar and midlatitude stratosphere [1,2]. Ozone-destroying Br is often formed in catalytic cycles that involve interhalogen reactions. The BrO + ClO reaction cycle in particular produces both Br and

Cl atoms to react with O_3. The reactivity of bromine on a per atom basis is approximately 70 times more destructive to stratospheric ozone than is chlorine [1,5,6].

$$Cl + O_3 \rightarrow ClO + O_2 \quad \text{(R1)}$$

$$Br + O_3 \rightarrow BrO + O_2 \quad \text{(R2)}$$

$$I + O_3 \rightarrow IO + O_2 \quad \text{(R3)}$$

The iodine-catalyzed destruction of O_3 is through IO, formed directly in the reaction between I atoms and O_3. Recent work suggested that iodine plays a more significant role than previously believed in stratospheric ozone chemistry and, moreover, that iodine is approximately 400–1000 times more effective at destroying ozone than stratospheric chlorine in the lower stratosphere. In the future, the share of halogen-induced ozone loss in the stratosphere due to reactions of iodine will likely be greater than it is today [7,8].

Of significant recent interest in the literature, and providing additional motivation for this work, is the potential for co-injection of inorganic halogens along with sulfate into the stratosphere from explosive volcanic eruptions [1,9]. While once believed to be unimportant due to hydrometeor scavenging, it is now well established that halogens from volcanoes are transported to the stratosphere, with recent enhancements in chlorine [10], bromine [11], and iodine [12] all being reported.

Gas-phase reactions involved in ozone loss cycles can have significant temperature dependences [13]. Hence, kinetic studies must be carried out over a wide range of temperatures to fully describe the behavior of these processes. In particular, extremely cold temperatures are possible in the upper troposphere and lower stratosphere. Largely because of their importance in stratospheric chemistry, the kinetics of O_3 reactions with halogen atoms have been the subject of numerous experimental studies (e.g., Cl + O_3, Br + O_3, and I + O_3) [14–37]. On the theoretical side, however, the number of kinetics studies of O_3 with halogen atoms are relatively sparse [38–46].

Farantos et al., 1978 [38] have studied the classical dynamics of the O_3 reaction with Cl and derived the rate coefficients from 220–300 K. Tyrrell et al., 2001 [40] have used B3 LYP/-311 + G* theories and found that the reaction between ozone and the Cl atom proceeds via an early transition state and a late transition state. Castillo et al., 2011 [41] have studied the dynamics of O_3 + Cl by means of quasi-classical trajectory (QCT) calculations using the UQCISD/aug-cc-pVDZ level of theory over the temperature range of 200–400 K. None of these studies used dual level calculations, which are known for more accurate kinetic parameters [47,48], especially at low temperatures. Very few groups have studied the reaction mechanism of O_3 with Br using theoretical methods [44–46], and theoretical rate coefficients have not been reported in the literature. While there are theoretical studies [49,50] of the reaction mechanism of O_3 with iodine oxides, there are no theoretical studies of the reaction mechanism and low temperature kinetics of O_3 with the I atom. To the best of our knowledge, the present study represents the first report of the theoretical temperature-dependent rate coefficients for the reactions of ozone with the bromine atom and the iodine atom.

The temperature ranges used to determine the recommended values in the most recent NASA/JPL [13] compendium for the reactions of O_3 with Cl, Br, and I atoms are 205–300 K, 195–422 K, and 230–370 K, respectively. The IUPAC [51]-recommended temperature ranges for the reactions of O_3 with Cl, Br, and I atoms are 180–300 K, 190–430 K, and 230–370 K, respectively. (Hereafter, NASA/JPL and IUPAC recommendations refer to [13,51], respectively, with superscript reference numbers not shown.) As the heterogeneous activation of inorganic chlorine primarily occurs when temperatures drop below ~195 K in the polar vortex, rate coefficients for the title reactions in the lower temperature range (especially < 200 K) are very important. The recommended temperature-dependent rate coefficients by both the NASA/JPL and IUPAC evaluations are limited, particularly for iodine. Both experimental and theoretical studies play important roles in improving our understanding of the chemical reactions that are occurring in the stratosphere, with theoretical calculations

in particular providing valuable mechanistic insight. Our focus here is to improve the theoretical understanding of the title reactions and extend the temperature range beyond what is experimentally available, from 180 to 400 K for all three halogens with a primary focus on atmospherically relevant conditions.

In the present investigation, the kinetics of O_3 with halogen atom reactions have been studied using canonical variational transition state theory including small curvature tunneling corrections (CVT/SCT) over the temperature range of 180–400 K. To get more constrained and accurate kinetics parameters, dual level calculations were performed at the MRCI + Q/aug-ano-pVTZ//MP2/aug-cc-pV(T + d)Z and MRCI + Q/aug-ano-RCC-VTZP//MP2/aug-cc-pV(T + d)Z levels of theory with ZORA (zeroth-order regular approximation) using the ORCA program. Thermodynamic properties were studied at the CCSD(T)/aug-cc-pV(T + d)Z level of theory. Reactivity trends of O_3 with all the halogens (F, Cl, Br, and I) and reaction pathways are discussed.

2. Computational Methods

The geometries and harmonic frequency calculations of reactants (halogens and O_3), pre-reactive complexes (PRCs), transition states (TSs), product complexes (PCs), and products were performed at the Møller−Plesset level of theory with second order perturbation (MP2) in combination with the augmented correlation consistent polarized triple-ζ (aug-cc-pV(T + d)Z) basis set [52,53]. Møller−Plesset perturbation theory assumes Hartee-Fock Hamiltonian as the zero-order perturbation. The combination of the MP2 method with the aug-cc-pV(T + d)Z basis set is extensively used for atmospheric reactions in the literature [54,55]. Transition states were identified with one imaginary frequency. Reactants, pre-reactive complexes, product complexes, and products were identified with zero imaginary frequencies. All the electronic structure calculations were performed using Gaussian 09 program suite [56], and all the normal modes and structures were viewed in Gauss view [57]. Intrinsic reaction coordinates (IRCs) calculations were carried out at the MP2/aug-cc-pV(T + d)Z level of theory for all the transition states to verify that the transition states are connected to the reactants and products. Thermodynamic properties were studied using Coupled-cluster with single, double, and triple excitation (CCSD(T)) with the aug-cc-pV(T + d)Z level of theory. To obtain more refrained and accurate energies, single point energy calculations were performed. Dual level calculations were carried out at the Multireference configuration interaction (MRCI) method. For better accuracy, the Davidson correction, core-valence correlation, and spin-orbit coupling effects are included (+Q). MRCI + Q in combination with aug-ano-pVTZ, aug-ano-RCC-VTZP, and ZORA (zeroth-order regular approximation) were used for refining energies [58,59]. These dual level calculations were performed using the ORCA program, which is one of the most versatile quantum chemistry packages available [60,61]. DFT, single-reference correlation, and multi-reference correlation methods can be executed using ORCA. The lowest spin-orbit states, A_1 for O_3 and $^2P_{3/2}$ for Cl, Br, and I atoms, were used throughout the calculations in this study.

3. Kinetics

The temperature-dependent rate coefficients for the reactions of halogen atoms with O_3 were calculated with CVT/SCT using the POLYRATE 2016A program and GAUSSRATE [62,63]. The POLYRATE program is a well-known software package for calculating kinetics parameters for gas-phase reactions; a detailed procedure was given in our previous articles [64,65]. To get the canonical variational transition state rate coefficient, the generalized rate coefficients can be minimized by varying the transition state dividing surface along the reaction coordinate using the following expressions:

$$k^{CVT/SCT}(T) = \mathrm{K}^{CVT/SCT}(T) k^{CVT}(T) \quad (1)$$

$$k^{GT}(T,s) = \sigma \frac{k_B T}{h} \left(\frac{Q^{GT}(T,s)}{\varnothing^R(T)} \right) exp\left(\frac{-V_{MEP}(s)}{k_B T} \right) \quad (2)$$

Here, $k^{CVT/SCT}(T)$ is the tunneling corrected rate coefficient, which is obtained by multiplying k^{CVT} and a temperature-dependent transmission coefficient $\kappa^{CVT/SCT}$, σ is reaction path degeneracy, k_B is Boltzmann's constant, T is temperature in Kelvin, h is Planck's constant. Q^{GT} is the canonical partition function of the generalized transition state at "s", and "s" is a reaction coordinate parameter that determines the location of the generalized transition dividing surface. $\varnothing^R$ is the partition function of the reactant. $V_{MEP}(s)$ is the potential along the reaction path at "s", and the minimum energy pathway (MEP) was constructed with a gradient step size of 0.01 Å. The canonical variational transition state is located by maximizing the free energy of activation with respect to "s". The minimum energy pathway is obtained using direct dynamics for a small range of the reaction path with the mass scaled reaction coordinate "s" from –1.0 to 1.0 Å by using the Page-McIver integrator with a step size of 0.01 Å.

4. Results and Discussion

4.1. Reaction of Cl + O_3

The potential energy level diagram for the reaction of O_3 with Cl atoms (R1) is given in Figure 1 along with the optimized geometries at the MP2/aug-cc-pV(T + d)Z level of theory. All the structural parameters are given in the Supplementary Materials Table S1. This reaction goes through an early transition state (pre-reactive complex, PRC), is connected through a late transition state (product complex, PC), and leads to the products as shown in Figure 1. The Cl atom attack on a terminal oxygen of the ozone in both trans and cis pathways was identified, consistent with previous literature [38–43]. Among the trans and cis pathways, the trans pathway was found to be the lowest energy pathway. Hence, the trans pathway is considered in the present kinetics calculations. In the case of O atom abstraction by the Cl atom, the breaking O–O bond length in O_3 was stretched up to 32% when compared with the bond length in the reactant O_3.

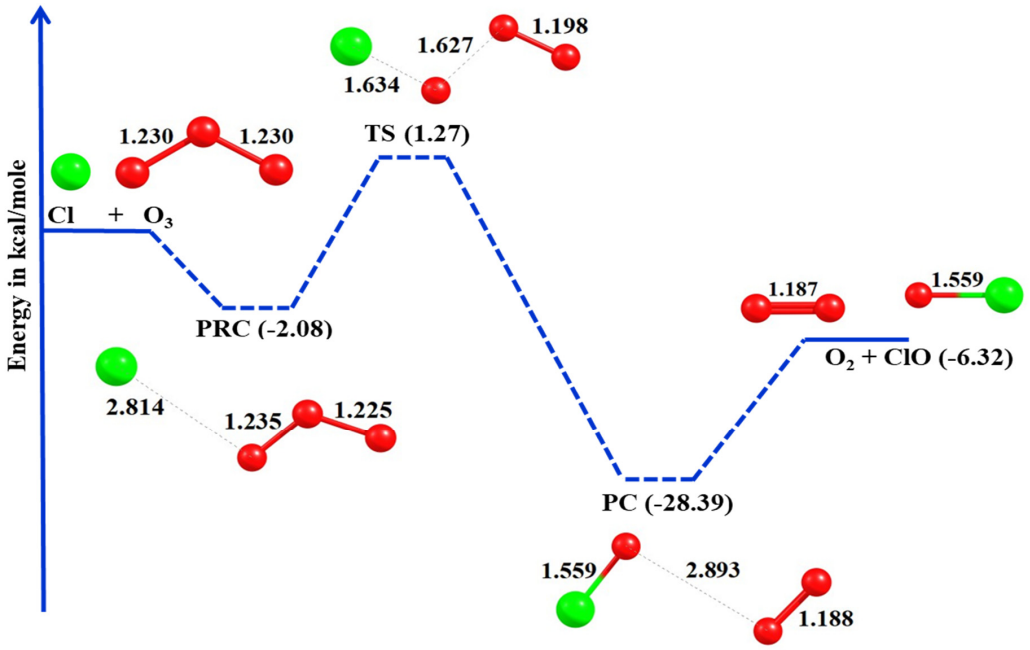

Figure 1. Potential energy level diagram for the reaction of O_3 with Cl obtained at the MRCI + Q/aug-ano-pVTZ//MP2/aug-cc-pV(T + d)Z levels of theory.

The obtained bond lengths, bond angles, and vibrational frequencies of the Cl + O_3 reaction in the present study are compared with values in the available literature in Tables 1 and 2. There is variation in the level of agreement across the 42 intercompared variables shown, but our computed bond lengths, bond angles, and vibrational frequencies typically agree with the reported values in previous studies. The observed differences are most likely due

to the different levels of theory and basis sets used in the computations by Hwang et al. [39] (QCISD/6-311G*), Tyrrell et al. [40] (PW91PW91/aug-cc-pVQZ and PW91PW91/6-311 + G*), and Castillo et al. [41] (QCISD/aug-cc-pVDZ) relative to the present study (MP2/aug-cc-pV(T + d)Z).

Table 1. The obtained bond lengths (r_e in Å) and bond angles (θ in deg) for the reaction of Cl + O_3 at various levels of theory.

Species		This Work	Hwang et al. [39]	Tyrrell et al. [40]		Castillo et al. [41]
		MP2/aug-cc-pV(T + d)Z	QCISD/6-311G*	pw91pw91/aug-cc-pVQZ	pw91pw91/6-311 + G*	QCISD/aug-cc-pVDZ
O_3	r_e	1.230	1.256	1.272	1.283	1.264
	θ	118.35	117.7	118.2	116.9	117.4
Pre-reactive complex	r_e Cl-O_1	2.814	2.284	2.305	2.313	2.449
	θ	101.2	110.8	110.8	112.4	109.5
	r_e O_1-O_2	1.235	1.320	1.323	1.336	1.315
	θ O_1-O_2-O_3	118.0	113.9	115.8	115.8	114.1
	r_e O_2-O_3	1.225	1.287	1.256	1.258	1.295
Transition state	r_e Cl-O_1	1.634	1.705	2.284	2.302	2.449
	θ	105.8	105.4	112.9	114.1	109.5
	r_e O_1-O_2	1.627	1.433	1.326	1.329	1.315
	θ O_1-O_2-O_3	108.6	107.7	118.7	118.7	114.1
	r_e O_2-O_3	1.198	1.239	1.254	1.256	1.295
Product complex	r_e Cl-O_1	1.559	1.664	1.642	1.637	2.449
	θ	106.0	106.2	111.3	112.9	109.5
	r_e O_1-O_2	2.893	1.625	2.441	2.191	1.315
	θ O_1-O_2-O_3	108.6	110.8	113.3	113.8	114.1
	r_e O_2-O_3	1.188	1.163	1.213	1.210	1.295
ClO	r_e Cl-O_1	1.559		1.53	1.619	1.634
O_2	r_e O_2-O_3	1.187		1.228	1.228	1.211

Table 2. Vibrational frequencies (cm^{-1}) for the reaction of Cl + O_3 at various levels of theory.

Species		This Work	Tyrrell et al. [40]	Castillo et al. [41]
		MP2/aug-cc-pV(T + d)Z	pw91pw91/aug-cc-pVQZ	QCISD/aug-cc-pVDZ
O_3	v_1	795.4	714	737
	v_2	1375.0	1066	894
	v_3	1379.9	1187	1219
Pre-reactive complex	v_1	39.8	83	
	v_2	87.0	157	
	v_3	95.3	252	
	v_4	800.6	558	
	v_5	1350.4	790	
	v_6	1394.1	1475	
Transition state	v_1	396.8*i*	134*i*	90*i*
	v_2	54.6	111	57
	v_3	231.2	211	187
	v_4	537.9	651	672
	v_5	861.0	818	867
	v_6	1520.8	1181	968
Product complex	v_1	43.5	40	
	v_2	63.1	54	
	v_3	101.3	123	
	v_4	113.8	150	
	v_5	792.3	822	
	v_6	1521.6	1538	
ClO	v_1	916.4	829	803
O_2	v_1	1765.3	1558	1625

The energies of all the stationary points were refined at MRCI + Q/aug-ano-pVTZ using the optimized geometries obtained at the MP2/aug-cc-pV(T + d)Z level of theory.

Thus, refined energies were used in dual level calculations to compute the rate coefficients for the reaction of R1 over the temperature range of 180–400 K. The rate coefficients from CVT/SCT at the MRCI + Q/aug-ano-pVTZ//MP2/aug-cc-pV(T + d)Z levels of theory are compared with the recommended rate coefficients by NASA/JPL and IUPAC in Figure 2. The obtained temperature-dependent rate coefficient (180–400 K) for R1 is $k_1 = (3.48 \pm 0.4) \times 10^{-11} \exp[(-301 \pm 64)/T]$ cm^3 molecule^{-1} s^{-1}. The reported uncertainties on the A factor and -E_a/R are, respectively, from the deviation in the intercept and slope of a two-parameter linear least squares fit of ln k versus 1/T. Table 3 shows the rate coefficients from this work compared with the recommended rate coefficients from NASA/JPL ($2.3 \times 10^{-11} \exp[-200/T]$ cm^3 molecule^{-1} s^{-1}) and IUPAC ($2.8 \times 10^{-11} \exp[-250/T]$ cm^3 molecule^{-1} s^{-1}).

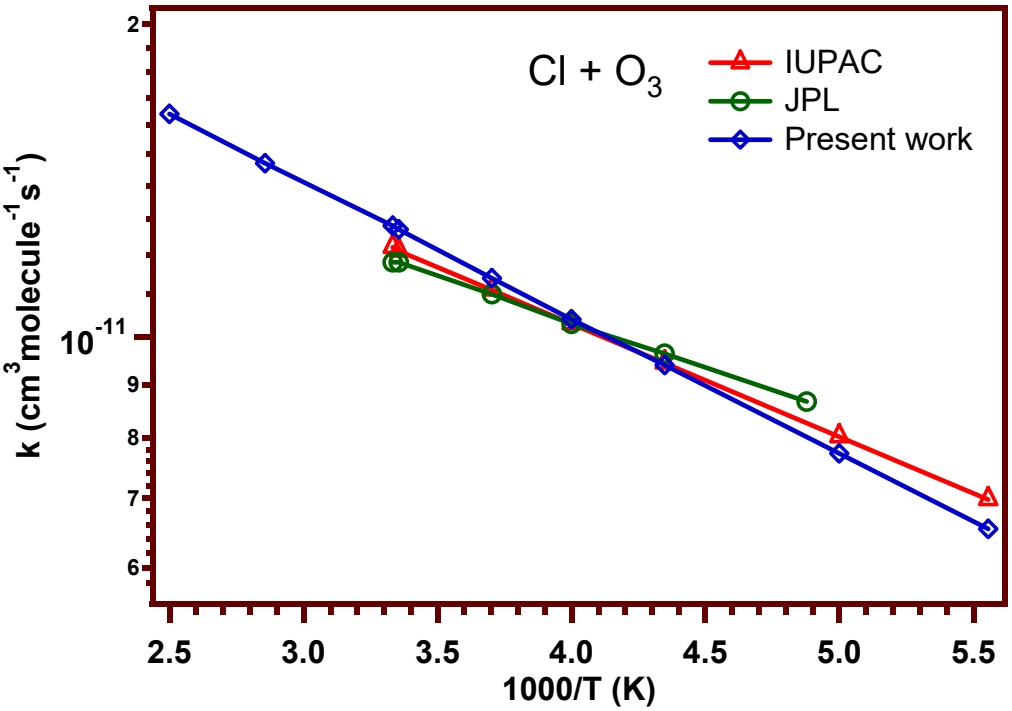

Figure 2. Arrhenius plot for the reaction of O_3 with Cl obtained at the MRCI + Q/aug-ano-pVTZ//MP2/aug-cc-pV(T + d)Z levels of theory using CVT/SCT rate coefficients in the temperature range of 180 and 400 K along with the recommended rate coefficients by NASA/JPL [13] and IUPAC [51].

Table 3. Rate coefficients (cm^3 molecule^{-1} s^{-1}) for the reaction of O_3 with Cl at the MRCI + Q/aug-ano-pVTZ//MP2/aug-cc-pV(T + d)Z levels of theory using CVT/SCT rate coefficients along with the recommended rate coefficients by NASA/JPL [13] and IUPAC [51] for comparison.

T(K)	k (Present Work)	k (JPL)	k (IUPAC)
180	6.54×10^{-12}		6.98×10^{-12}
200	7.73×10^{-12}		8.02×10^{-12}
210	8.30×10^{-12}	8.87×10^{-12}	8.51×10^{-12}
230	9.40×10^{-12}	9.64×10^{-12}	9.44×10^{-12}
250	1.04×10^{-11}	1.03×10^{-11}	1.03×10^{-12}
270	1.14×10^{-11}	1.10×10^{-11}	1.11×10^{-11}
298	1.27×10^{-11}	1.18×10^{-11}	1.21×10^{-11}
300	1.28×10^{-11}	1.18×10^{-11}	1.22×10^{-11}
350	1.47×10^{-11}		
400	1.64×10^{-11}		

The obtained rate coefficients in the present study for the reaction of R1 are in excellent agreement with the JPL- and IUPAC-recommended values, differing by only 7% and 5%,

respectively, at 298 K. For comparison, the theoretically reported rate coefficient at 298 K by Farantos et al. (2.6×10^{-11} cm^3 $molecule^{-1}$ s^{-1}) is a factor of two higher than the recommended rate coefficient by the NASA/JPL evaluation, and the 298 K value of Castillo et al. (9.29×10^{-12} cm^3 $molecule^{-1}$ s^{-1}) is 21% lower. Our rate coefficients differ by 0–8% over the temperature range of 205–300 K when compared with JPL-recommended values and by 0–7% from 180–300 K when compared with IUPAC. Overall, the obtained rate coefficients in the present investigation are very close to the NASA/JPL and IUPAC-recommended rate coefficients when compared with previously reported theoretical rate coefficients, which shows the accuracy and reliability of the advanced theoretical methods used in the present calculations.

Further comparison of our theoretical rate coefficients with previous individual experimental studies generally yields good agreement. The obtained rate coefficients for the reaction of R1 differ by 0–4% when compared with Beach et al. [14] ($(3.1 \pm 1.35) \times 10^{-11}$ exp[–(280 ± 100)/T] cm^3 $molecule^{-1}$ s^{-1}) over the temperature range of 184–298 K, 14–15% when compared with Kurylo and Braun [21] ($(2.94 \pm 0.49) \times 10^{-11}$ exp[$-(298 \pm 39)$/T] cm^3 $molecule^{-1}$ s^{-1}) over the temperature range of 213–298 K, 4% when compared with Leu and DeMore [22] ($(1.3 \pm 0.3) \times 10^{-11}$ cm^3 $molecule^{-1}$ s^{-1}) at 295 K, 7–15% when compared with Nicovich et al. [23] ($(2.49 \pm 0.38) \times 10^{-11}$ exp[$-(233 \pm 46)$/T] cm^3 $molecule^{-1}$ s^{-1}) over the temperature range of 264–385 K, 0–30% when compared with Seely et al. [24] ($(1.63 \pm 0.34) \times 10^{-11}$ exp[$-(91 \pm 61)$/T] cm^3 $molecule^{-1}$ s^{-1}) over the temperature range of 206–296 K, and 0–25% when compared with Zahniser et al. [27] ($(2.35 \pm 0.5) \times 10^{-11}$ exp[$-(171 \pm 30)$/T] cm^3 $molecule^{-1}$ s^{-1}) over the temperature range of 210–360 K.

4.2. Reaction of Br + O_3

The potential energy level diagram for the reaction of O_3 with Br atoms (R2) is given in Figure 3 along with the optimized geometries at the MP2/aug-cc-pV(T + d)Z level of theory. All the structural parameters are given in the Supplementary Materials Table S2. This reaction goes through an early transition state (pre-reactive complex, PRC), is connected through a late transition state (product complex, PC), and leads to the products as shown in Figure 3. The Br atom attack on a terminal oxygen of the ozone in both trans and cis pathways was identified analogously to reaction R1. Among the trans and cis pathways, the trans pathway was found to be the lowest energy pathway. Hence, the trans pathway is considered in the present kinetics calculations. In the case of O atom abstraction by the Br atom, the breaking O–O bond length in O_3 was stretched up to 34% when compared with the bond length in the reactant O_3.

The obtained bond lengths, bond angles, and vibrational frequencies of the Br + O_3 reaction in the present study are shown, along with values from previous studies in Tables 4 and 5. When compared with Bing et al. [45] and A-Hussein et al. [46], our results represent the first reported values for the product complex of the Br + O_3 reaction. Where intercomparison with existing literature is possible, the computed bond lengths, bond angles, and vibrational frequencies exhibit some variation but are typically in agreement. The observed differences are most likely due to the different levels of theory and basis sets used in the computations by Bing et al. [45] (MP2/6-311 + G(d)) and A-Hussein et al. [46] (PM3-CI) relative to the present study (MP2/aug-cc-pV(T + d)Z).

The energies of all the stationary points were refined at MRCI + Q/aug-ano-RCC-VTZP using the optimized geometries obtained at the MP2/aug-cc-pV(T + d)Z level of theory. Thus, refined energies were used in dual level calculations to compute the rate coefficients for the reaction of R2 over the temperature range of 180–400 K. The obtained rate coefficients from CVT/SCT at the MRCI + Q/aug-ano-RCC-VTZP//MP2/aug-cc-pV(T + d)Z levels of theory are compared with the recommended rate coefficients by NASA/JPL and IUPAC in Figure 4. The rate coefficients from CVT/SCT were used to fit the Arrhenius expression, and the obtained temperature-dependent rate coefficient (180–400 K) for R2 is $k_2 = (3.54 \pm 0.2) \times 10^{-11}$ exp[(-990 ± 35)/T] cm^3 $molecule^{-1}$ s^{-1}. The reported uncertainties on the A factor and $-E_a/R$ are, respectively, from the deviation

in the intercept and slope of a two-parameter linear least squares fit of ln k versus 1/T. Table 6 shows the rate coefficients from this work compared with the recommended rate coefficients from NASA/JPL (1.6×10^{-11} exp[−780/T] cm^3 $molecule^{-1}$ s^{-1}) and IUPAC (1.7×10^{-11} exp[−800/T] cm^3 $molecule^{-1}$ s^{-1}).

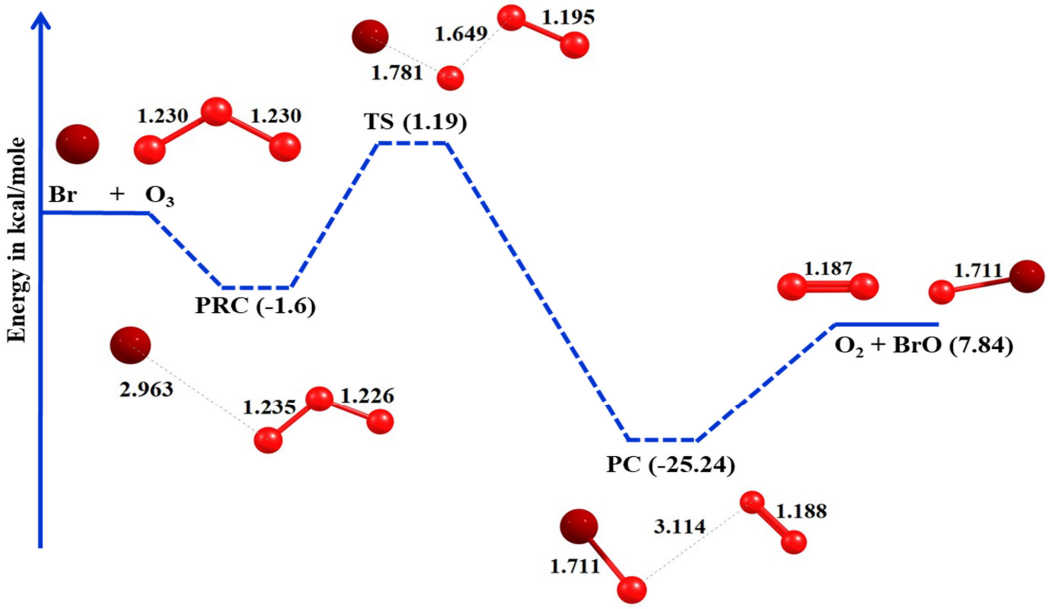

Figure 3. Potential energy level diagram for the reaction of O_3 with Br obtained at the MRCI + Q/aug-ano-RCC-VTZP//MP2/aug-cc-pV(T + d)Z levels of theory.

Table 4. The obtained bond lengths (r_e in Å) and bond angles (θ in deg) for the reaction of Br + O_3 at various levels of theory.

Species		This Work	Bing et al. [45]	A-Hussein et al. [46]
		MP2/aug-cc-pV (T + d)Z	MP2/6-31G(d)	PM3-CI (4 × 4)
O_3	r_e	1.230	1.300	
	θ	118.3	116.8	
Pre-reactive complex	r_e Br-O_1	2.963	2.655	2.981
	θ	102.2	107.5	107.31
	r_e O_1-O_2	1.235	1.311	1.937
	θ O_1-O_2-O_3	118.0	113.0	116.86
	r_e O_2-O_3	1.226	1.305	1.172
Transition state	r_e Br-O_1	1.781	2.248	2.357
	θ	106.4	108.4	104.7
	r_e O_1-O_2	1.649	1.434	1.627
	θ O_1-O_2-O_3	108.6	111.1	103.8
	r_e O_2-O_3	1.195	1.276	1.191
Product complex	r_e Br-O_1	1.711		
	θ	84.4		
	r_e O_1-O_2	3.114		
	θ O_1-O_2-O_3	85.9		
	r_e O_2-O_3	1.188		
BrO	r_e Br-O_1	1.711	1.753	
O_2	r_e O_2-O_3	1.187	1.247	

Table 5. Vibrational frequencies (cm^{-1}) for the reaction of Br + O_3 at various levels of theory.

Species		This Work	Bing et al. [45]	
		MP2/aug-cc-pV (T + d)Z	MP2/6-31G(d)	MP2/6-311 + G(d)
O_3	v_1	795.4		
	v_2	1375.0		
	v_3	1379.9		
Pre-reactive complex	v_1	53.2	84.3	60.2
	v_2	91.7	315.7	321.6
	v_3	112.7	645.3	653.7
	v_4	802.1	960.5	953.9
	v_5	1351.3	1184.0	1213.9
	v_6	1394.7	2145.8	1988.9
Transition state	v_1	476.6*i*	55.7*i*	
	v_2	61.2	56.4	
	v_3	200.7	181.9	
	v_4	456.0	679.6	
	v_5	768.4	1035.1	
	v_6	1539.6	1063.0	
Product complex	v_1	39.5		
	v_2	45.8		
	v_3	83.0		
	v_4	93.5		
	v_5	778.7		
	v_6	1765.1		
BrO	v_1	791.9	765.4	750.6
O_2	v_1	1765.3		

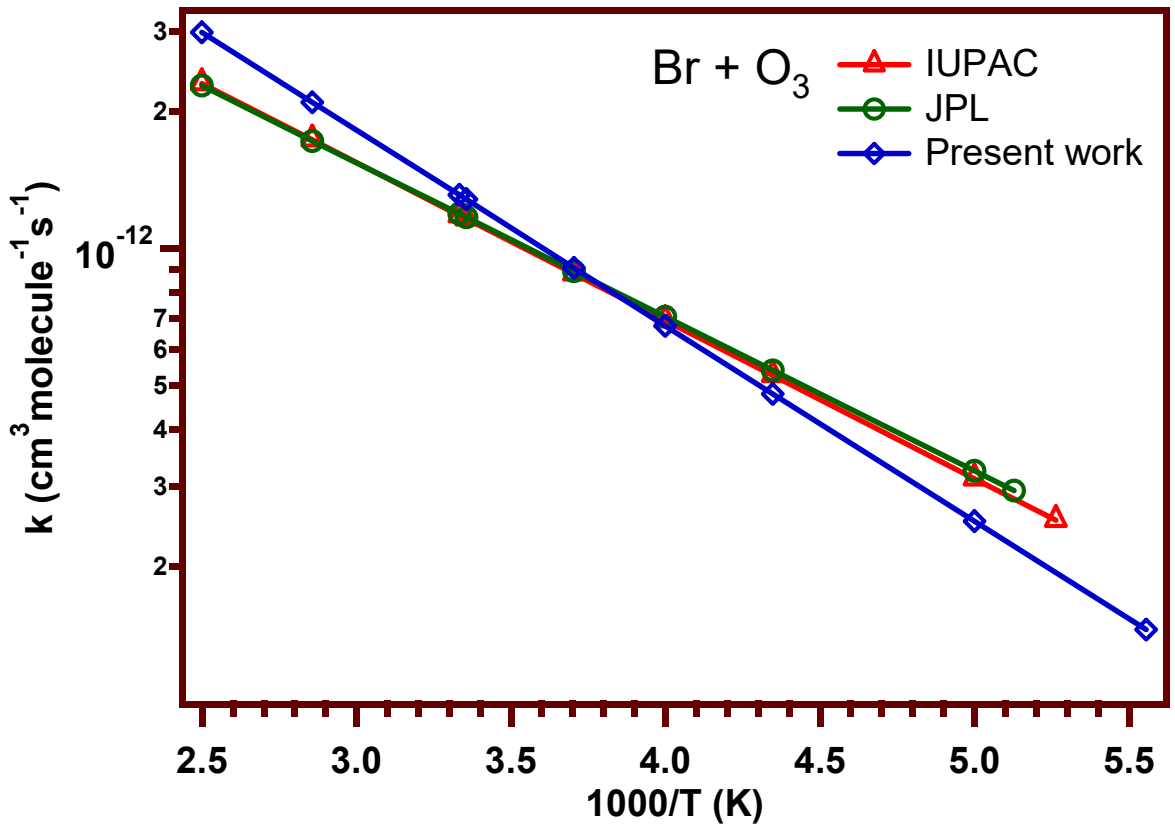

Figure 4. Arrhenius plot for the reaction of O_3 with Br obtained at the MRCI + Q/aug-ano-RCC-VTZP//MP2/aug-cc-pV (T + d)Z levels of theory using CVT/SCT rate coefficients in the temperature range of 180 and 400 K along with the recommended rate coefficients by NASA/JPL [13] and IUPAC [51].

Table 6. Rate coefficients (cm^3 $molecule^{-1}$ s^{-1}) for the reaction of O_3 with Br at the MRCI + Q/aug-ano-RCC-VTZP//MP2/aug-cc-pV(T + d)Z levels of theory using CVT/SCT along with the recommended rate coefficients by NASA/JPL [13] and IUPAC [51] for comparison.

T (K)	k (Present Work)	k (JPL)	k (IUPAC)
180	1.45×10^{-13}		
200	2.51×10^{-13}	3.24×10^{-13}	3.11×10^{-13}
230	4.78×10^{-13}	5.39×10^{-13}	5.25×10^{-13}
250	6.75×10^{-13}	7.07×10^{-13}	6.93×10^{-13}
270	9.05×10^{-13}	8.90×10^{-13}	8.78×10^{-13}
298	1.28×10^{-12}	1.17×10^{-12}	1.16×10^{-12}
300	1.31×10^{-12}	1.19×10^{-12}	1.18×10^{-12}
350	2.09×10^{-12}	1.72×10^{-12}	1.73×10^{-12}
400	2.98×10^{-12}	2.28×10^{-12}	2.30×10^{-12}

The obtained rate coefficient for the reaction of R2 at 298 K differs by 9% when compared with either the NASA/JPL-recommended value or IUPAC. As stated previously, there are no theoretical rate coefficients in the literature to compare with the obtained rate coefficients in the present study. Our rate coefficients differ by 0–33% over the temperature range of 195–400 K when compared with JPL-recommended values and by 0–31% from 190–400 K when compared with IUPAC. Our rate coefficients are smaller than the recommended rate coefficients in the temperature range of 195–250 K and larger in the temperature range of 250–400 K. The level of agreement is within the stated uncertainty range of the NASA/JPL and IUPAC recommendations and the uncertainty range of the present calculations.

Further comparison of our theoretical rate coefficients with previous individual experimental studies generally yields good agreement. The obtained rate coefficients using CVT/SCT for the reaction of R2 differ by maximum of 0–3% when compared with Leu and DeMore [29] ($(3.34 \pm 0.40) \times 10^{-11}$ $\exp[-(978 \pm 36)/T]$ cm^3 $molecule^{-1}$ s^{-1}) over the temperature range of 224−400 K, 0–33% when compared with Michael and Payne [31] ($(9.45 \pm 2.48) \times 10^{-12}$ $\exp[-(659 \pm 64)/T]$ cm^3 $molecule^{-1}$ s^{-1}) over the temperature range of 234−360 K, 6% when compared with Ninomiya et al.[32] ($(1.2 \pm 0.1) \times 10^{-12}$ cm^3 $molecule^{-1}$ s^{-1}) at 298 K, and 4–12% when compared with Toohey et al.[33] ($(3.28 \pm 0.40) \times 10^{-11}$ $\exp[-(944 \pm 30)/T]$ cm^3 $molecule^{-1}$ s^{-1}) over the temperature range of 248–400 K.

4.3. Reaction of I + O_3

The potential energy level diagram for the reaction of O_3 with I atoms (R3) is given in Figure 5 along with the optimized geometries at the MP2/aug-cc-pV(T + d)Z level of theory. All the structural parameters for the reaction of R3 are given in the Supplementary Materials Table S3. This reaction goes through an early transition state (pre-reactive complex, PRC), is connected through a late transition state (product complex, PC), and leads to the products as shown in Figure 5. Both trans and cis pathways for the I atom attack on a terminal oxygen of the ozone were identified analogously to reactions (R1) and (R2). Among the trans and cis pathways, the trans pathway was found to be the lowest energy pathway. Hence, the trans pathway is considered in the present kinetics calculations. In the case of O atom abstraction by the I atom, the breaking O–O bond length in O_3 was stretched up to 36% when compared with the bond length in the reactant O_3.

The obtained bond lengths, bond angles, and vibrational frequencies in the present study are shown in Tables 7 and 8 and are compared with the limited available literature data where possible. With all but two exceptions, our data represent the first reported values. Our computed I–O bond length is very close to the reported I–O bond length by Papayannis et al. [54] and our computed IO vibrational frequency is slightly higher than the reported value by Papayannis et al. [54]. The observed differences are most likely due to the different level of basis set used in the computations of IO by Papayannis et al. [54] (MP2/LANL2DZ) relative to the present study (MP2/aug-cc-pV(T + d)Z).

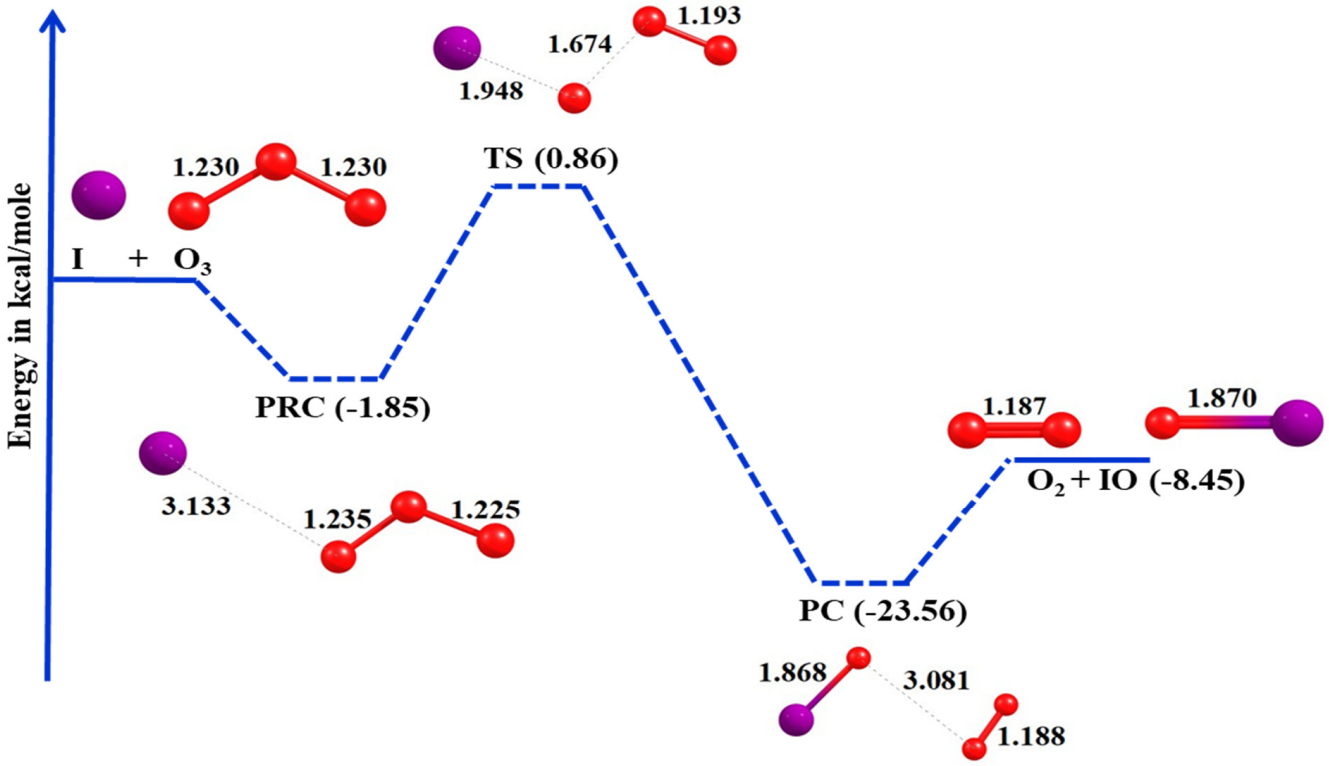

Figure 5. Potential energy level diagram for the reaction of O_3 with I obtained at the MRCI + Q/aug-ano-RCC-VTZP//MP2/aug-cc-pV(T + d)Z levels of theory.

The energies of all the stationary points were refined at MRCI + Q/aug-ano-RCC-VTZP using the optimized geometries obtained at the MP2/aug-cc-pV(T + d)Z level of theory. Thus, refined energies were used in dual level calculations to compute the rate coefficients for the reaction of R3 over the temperature range of 180–400 K. The rate coefficients obtained in the present study for the reaction of R3 at the MRCI + Q/aug-ano-RCC-VTZP//MP2/aug-cc-pV(T + d)Z levels of theory are compared with the recommended rate coefficients by NASA/JPL and IUPAC in Figure 6. The rate coefficients from CVT/SCT were used to fit the Arrhenius expression, and the obtained temperature-dependent rate coefficient (180–400K) for R3 is $k_3 = (1.47 \pm 0.1) \times 10^{-11}\exp[(-720 \pm 42)/T]$ cm^3 molecule^{-1}s^{-1}. The reported uncertainties on the A factor and -E_a/R are, respectively, from the deviation in the intercept and slope of a two-parameter linear least squares fit of ln k versus 1/T. Table 9 shows the rate coefficients from this work compared with the recommended rate coefficients from NASA/JPL ($2.0 \times 10^{-11}\exp[-830/T]$ cm^3 molecule^{-1}s^{-1}) and IUPAC ($2.1 \times 10^{-11}\exp[-830/T]$ cm^3 molecule^{-1}s^{-1}).

Our rate coefficient at 298 K is in very good agreement with the JPL- and IUPAC-recommended values, differing by 6% and 1%, respectively. There are no previous theoretical studies available for the reaction of R3 to compare with the obtained rate coefficients in the present study. This work provides rate coefficient data at significantly colder temperatures than in the NASA/JPL and IUPAC recommendations. For the overlapping temperature ranges, our rate coefficients agree within 0–16% relative to the NASA/JPL recommendation (230–370 K) and within 0–11% relative to IUPAC (230–370 K). The level of agreement at all temperatures is within the stated uncertainty range of the NASA/JPL and IUPAC recommendations and the uncertainty range of the present calculations.

Table 7. The obtained bond lengths (r_e in Å) and bond angles (θ in deg) for the reaction of I + O_3.

Species		This Work	Papayannis et al. [54]
		MP2/aug-cc-pV (T + d)Z	MP2/LANL2DZ
O_3	r_e	1.230	
	θ	118.3	
Pre-reactive complex	r_e I-O_1	3.133	
	θ	109.9	
	r_e O_1-O_2	1.235	
	θ O_1-O_2-O_3	118.1	
	r_e O_2-O_3	1.225	
Transition state	r_e Cl-O_1	1.948	
	θ	107.4	
	r_e O_1-O_2	1.674	
	θ O_1-O_2-O_3	108.9	
	r_e O_2-O_3	1.193	
Product complex	r_e I-O_1	1.868	
	θ	92.5	
	r_e O_1-O_2	3.081	
	θ O_1-O_2-O_3	83.9	
	r_e O_2-O_3	1.188	
IO	r_e I-O_1	1.870	1.877
O_2	r_e O_2-O_3	1.187	

Table 8. Vibrational frequencies (cm^{-1}) for the reaction of I + O_3.

Species		This Work	Papayannis et al. [54]
		MP2/aug-cc-pV (T + d)Z	MP2/LANL2DZ
O_3	v_1	795.4	
	v_2	1375.0	
	v_3	1379.9	
Pre-reactive complex	v_1	48.0	
	v_2	77.5	
	v_3	94.6	
	v_4	801.5	
	v_5	1355.1	
	v_6	1395.7	
Transition state	v_1	527.3*i*	
	v_2	65.3	
	v_3	183.9	
	v_4	418.6	
	v_5	718.4	
	v_6	1554.4	
Product complex	v_1	37.4	
	v_2	58.4	
	v_3	93.6	
	v_4	120.0	
	v_5	678.9	
	v_6	1768.2	
IO	v_1	662.7	597
O_2	v_1	1765.3	

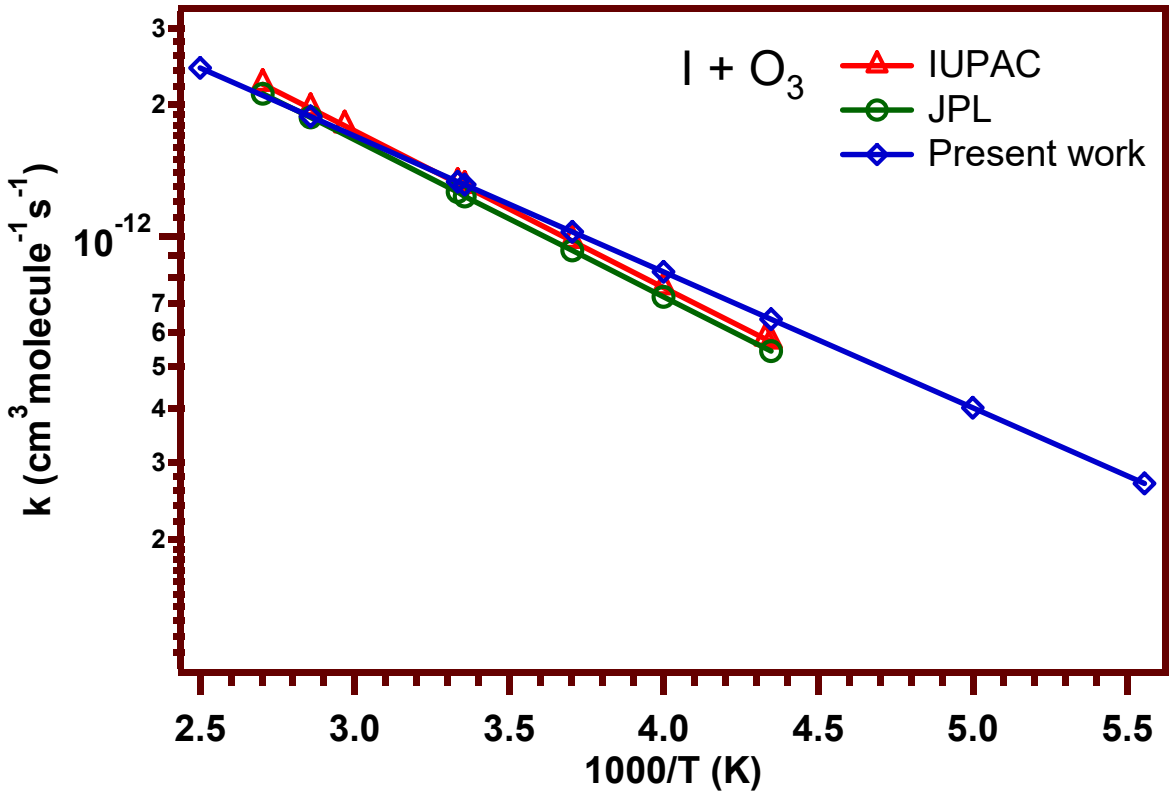

Figure 6. Arrhenius plot for the reaction of O_3 with I obtained at the MRCI + Q/aug-ano-RCC-VTZP//MP2/aug-cc-pV(T + d)Z levels of theory using CVT/SCT rate coefficients in the temperature range of 180 and 400 K along with the recommended rate coefficients by NASA/JPL [13] and IUPAC [51].

Table 9. Rate coefficients ($cm^3molecule^{-1}s^{-1}$) for the reaction of O_3 with I at the MRCI + Q/aug-ano-RCC-VTZP//MP2/aug-cc-pV(T + d)Z levels of theory using CVT/SCT along with the recommended rate coefficients by NASA/JPL [13] and IUPAC [51] for comparison.

T (K)	k (Present Work)	k (JPL)	k (IUPAC)
180	2.69×10^{-13}		
200	4.02×10^{-13}		
230	6.42×10^{-13}	5.42×10^{-13}	5.69×10^{-13}
250	8.25×10^{-13}	7.23×10^{-13}	7.59×10^{-13}
270	1.02×10^{-12}	9.25×10^{-13}	9.71×10^{-13}
298	1.31×10^{-12}	1.23×10^{-12}	1.30×10^{-12}
300	1.33×10^{-12}	1.26×10^{-12}	1.32×10^{-12}
350	1.88×10^{-12}	1.87×10^{-12}	1.96×10^{-12}
400	2.43×10^{-12}		

Further comparison of our theoretical rate coefficients with previous individual experimental studies generally yields good agreement. The obtained temperature-dependent rate coefficients in the present study for the reaction of R3 differ by 0–13% when compared with Turnipseed et al. [37] $((2.3 \pm 0.7) \times 10^{-11}\exp[-(860 \pm 100)/T]$ cm^3 $molecule^{-1}s^{-1})$ over the available temperature range of 240–370K. The obtained rate coefficient for the reaction of R3 differs by 2% and 28% at 298 K when compared with Tucceri et al. [35] $((1.28 \pm 0.06) \times 10^{-12}$ $cm^3molecule^{-1}s^{-1})$ and Sander [36] $((9.5 \pm 1.5) \times 10^{-13}$ $cm^3molecule^{-1}s^{-1})$, respectively.

4.4. Feasibility of the Reactions

To understand the feasibility and spontaneity of the reactions R1, R2, and R3 in terms of thermodynamic parameters, the enthalpies (Δ_rH°, kcal mol^{-1}), Gibbs free energies (Δ_rG°, kcal mol^{-1}), and entropies (Δ_rS°, cal mol^{-1} K^{-1}) at different levels of theory and

basis sets are collected in Table 10 along with reported values in the literature at 298K. Our obtained enthalpy for the reaction of R1 at CCSD(T)/aug-cc-pV(T + d)Z (−36.01 kcal/mol) is within 8% of the recommended value by the IUPAC evaluation (−38.81 kcal/mol) and the experimental value of Molina and Rowland [66] (−38.9 kcal/mol), and within 1% of the mean theoretical value from Hwang et al. [39] using G2MP2 and G2MP2 with higher level correction (−35.95 kcal/mol). Our obtained enthalpy for the reaction of R2 at CCSD(T)/aug-cc-pV(T + d)Z (−31.22 kcal/mol) is within 3% of the recommended value by the IUPAC evaluation (−32.26 kcal/mol) and the experimental value of Dyke et al. [67] (−32.3 kcal/mol), and within 4% of the mean theoretical value from Bing et al. [45] and A-Hussein et al. [46] using CCSD(T)/6-311 + G(3df), G2MP2, and PM3-CI (−32.38 kcal/mol). Our obtained Gibbs free energy for the reaction of R2 at CCSD(T)/aug-cc-pV(T + d)Z (−32.65 kcal/mol) is within 5% of the mean theoretical value from Bing et al. [45] and A-Hussein et al. [46] (−34.41 kcal/mol). Finally, our obtained enthalpy for the reaction of R3 at CCSD(T)/aug-cc-pV(T + d)Z (−29.86 kcal/mol) is within 7% of the recommended value by the IUPAC evaluation (−32.02 kcal/mol). There are no previous theoretical studies available for the reaction of R3 to compare with the obtained values in the present study.

Table 10. Enthalpies ($\Delta_rH°$, kcal mol^{-1}), Gibbs free energies ($\Delta_rG°$, kcal mol^{-1}) and entropies ($\Delta_rS°$, cal mol^{-1} K^{-1}) for the reactions of O_3 with Cl, Br, and I atoms obtained at various levels of theory along with the reported values in the literature at 298 K.

	Cl + O_3			**Br + O_3**			**I + O_3**		
	$\Delta_rH°$	$\Delta_rG°$	$\Delta_rS°$	$\Delta_rH°$	$\Delta_rG°$	$\Delta_rS°$	$\Delta_rH°$	$\Delta_rG°$	$\Delta_rS°$
[a] CCSD(T)/aug-cc-pV(T + d)Z	−36.01	−37.54	4.62	−31.22	−32.65	4.99	−29.86	−31.01	5.34
IUPAC[51]	−38.81			−32.26			−32.02		
[b] Experimental	−38.9								
[c] G2MP2	−37.5								
[c] G2MP2 with HLC	−34.4								
[d] Experimental				−32.3					
[e] CCSD(T)/6-311 + G(3df)				−33.54	−35.67				
[e] G2MP2				−26.70	−29.01				
[f] PM3-CI				−36.9	−38.55				

[a] This work, [b] Molina and Rowland [66], [c] Hwang et al. [39], [d] Dyke et al. [67], [e] Bing et al. [45], and [f] A-Hussein et al. [46].

In addition to the data comparisons above, we provide a number of new thermodynamic parameters in Table 10 not previously reported in the literature to our knowledge. Based on the results in Table 10, the O atom abstractions by halogen atoms are feasible and spontaneous. Among these halogens, Cl atom abstraction reactions are more feasible and spontaneous than the Br and I atom abstraction reactions both kinetically and thermodynamically, which is consistent with the present kinetics findings.

4.5. Kinetics Analysis

From Figures 2, 4 and 6, it is clear that the reactions of R1, R2, and R3 show positive temperature dependencies, which is consistent with the NASA/JPL and IUPAC evaluations over the studied temperature range (180–400 K). Table 11 shows that the room temperature (298 K) rate coefficient for the reaction of O_3 with F atoms is close to that of the reaction of O_3 with Cl atoms. Similarly, the room temperature (298 K) rate coefficient for the reaction of O_3 with Br atoms is close to that of the rate coefficient for the reaction of O_3 with I atoms. In addition, both the theory results from this work and the NASA/JPL recommendation show that the rate coefficient for the reaction of O_3 with Cl atoms is approximately a factor of 10 faster than the reaction of O_3 with Br or I atoms at 298 K. This may be explained based on pre-exponential factors and activation energies listed in Table 11; in particular, it is clear that the activation energy for the reaction of O_3 with a Cl atom is significantly lower than the activation energies of reactions of O_3 with Br and I atoms.

Table 11. Rate coefficients at 298 K ($cm^3molecule^{-1}s^{-1}$), pre-exponential factors ($cm^3molecule^{-1}s^{-1}$), and activation energies/R (K) for the reactions of O_3 with F, Cl, Br, and I atoms.

Reaction	k [a]	A [a]	E_a/R [a]	k [b]	A [b]	E_a/R [b]
$F + O_3$				1.0×10^{-11}	2.2×10^{-11}	230
$Cl + O_3$	1.27×10^{-11}	3.48×10^{-11}	301	1.18×10^{-11}	2.3×10^{-11}	200
$Br + O_3$	1.28×10^{-12}	3.54×10^{-11}	990	1.17×10^{-12}	1.6×10^{-11}	780
$I + O_3$	1.31×10^{-12}	1.47×10^{-11}	720	1.23×10^{-12}	2.0×10^{-11}	830

[a] Results from this work. [b] NASA/JPL [13] recommended values.

The obtained rate coefficients in the present study for the title reactions are very close to the recommended rate coefficients by NASA/JPL and IUPAC evaluations in the vicinity of room temperature (298 K). When the temperature range is extended to substantially colder and warmer temperatures, the rate coefficients deviate farther from the recommended rate coefficients by the NASA/JPL and IUPAC evaluations but are still in agreement within uncertainty. The overall consistency between our calculated values and the previous experimental studies supports the accuracy of the results presented here, which in turn, helps underpin the theoretical foundation of the $X + O_3$ title reactions over the considered temperature range.

5. Conclusions

In this study, the reactions of O_3 with Cl, Br, and I atoms were investigated using canonical variational transition state theory including small curvature tunneling corrections (CVT/SCT). Rate coefficients were computed at MRCI + Q/aug-ano-pVTZ//MP2/aug-cc-pV(T + d)Z and MRCI + Q/aug-ano-RCC-VTZP//MP2/aug-cc-pV(T + d)Z levels of theory. To our knowledge, this study represents the first reported temperature-dependent rate coefficients for the reactions of O_3 with Br and I using theoretical methods. Dual level calculations give more accurate and refined kinetics parameters, which had not been performed previously in the literature for any of the title reactions. The temperature range is also extended relative to previous experimental studies for the three reactions from 180 to 400 K. Overall, we find very good agreement between our temperature-dependent rate coefficients and the experimentally derived, recommended values from NASA/JPL and IUPAC for the three $X + O_3$ reactions studied here, thereby helping underpin the theoretical foundation for these important ozone-loss reactions. The reaction of O_3 with the iodine atom proceeds via an early transition state and a late transition state, which is analogous to reactions of O_3 with Cl and Br but had not previously been reported in the literature. Thermodynamically, these three reactions are feasible and spontaneous. Previous experimental values and our theoretical results show that the reaction of Cl atoms with O_3 is around a factor of 10 times faster than the reactions of O_3 with Br and I atoms.

Supplementary Materials: The following are available online at https://www.mdpi.com/article/10.3390/atmos12081053/s1, Table S1: Optimized geometries of the reactants, pre-reactive complex, transition state, product complex, and products at the MP2/aug-cc-pV(T + d)Z level of theory for the reaction of O_3 with the Cl atom, Table S2: Optimized geometries of the reactants, pre-reactive complex, transition state, product complex, and products at the MP2/aug-cc-pV(T + d)Z level of theory for the reaction of O_3 with the Br atom, Table S3: Optimized geometries of the reactants, pre-reactive complex, transition state, product complex, and products at the MP2/aug-cc-pV(T + d)Z level of theory for the reaction of O_3 with the I atom.

Author Contributions: Conceptualization, S.V. and D.M.W.; methodology, S.V. and D.S.R.; software, S.V. and D.S.R.; validation, S.V.; formal analysis, S.V., D.S.R. and D.M.W.; investigation, S.V.; data curation, S.V.; writing—original draft preparation, S.V.; writing—review and editing, D.M.W.; visualization, S.V.; supervision, D.M.W.; funding acquisition, D.M.W. All authors have read and agreed to the published version of the manuscript.

Funding: The authors gratefully acknowledge funding support from the National Aeronautics and Space Administration (NASA) through grant numbers 80NSSC18K1063 and NNX15AD87G. The APC was funded by NASA grant number 80NSSC18K1063.

Institutional Review Board Statement: Not applicable.

Informed Consent Statement: Not applicable.

Data Availability Statement: Data used in this publication are available in the Tables of the manuscript and in the Supplementary Materials.

Acknowledgments: We thank James G. Anderson, Stephen J. Klippenstein, John R. Barker, Theodore S. Dibble, and William H. Green for their assistance during this work. We acknowledge computer support from the Research Computing Center at Harvard University.

Conflicts of Interest: The authors declare no conflict of interest.

References

1. World Meteorological Organization (WMO). *Scientific Assessment of Ozone Depletion: 2018*; Global Ozone Research and Monitoring Project–Report No. 58; World Meteorological Organization (WMO): Geneva, Switzerland, 2018.
2. Wilmouth, D.M.; Salawitch, R.J.; Canty, T.P. Stratospheric ozone depletion and recovery. In *A Chapter in Green Chemistry: An Inclusive Approach*; Torok, B., Dransfield, T., Eds.; Elsevier Publishing: Amsterdam, The Netherlands, 2018; pp. 177–209.
3. Molina, L.T.; Molina, M.J. Production of Cl_2O_2 from the self-reaction of the ClO radical. *J. Phys. Chem.* **1987**, *91*, 433–436. [CrossRef]
4. Wilmouth, D.M.; Hanisco, T.F.; Stimpfle, R.M.; Anderson, J.G. Chlorine-catalyzed ozone destruction: Cl atom production from ClOOCl photolysis. *J. Phys. Chem. A* **2009**, *113*, 14099–14108. [CrossRef] [PubMed]
5. Sinnhuber, B.M.; Sheode, N.; Sinnhuber, M.; Chipperfield, M.P.; Feng, W. The contribution of anthropogenic bromine emissions to past stratospheric ozone trends: A modelling study. *Atmos. Chem. Phys.* **2009**, *9*, 2863–2871. [CrossRef]
6. Klobas, J.E.; Weisenstein, D.K.; Salawitch, R.J.; Wilmouth, D.M. Reformulating the bromine alpha factor and equivalent effective stratospheric chlorine (EESC): Evolution of ozone destruction rates of bromine and chlorine in future climate scenarios. *Atmos. Chem. Phys.* **2020**, *20*, 9459–9471. [CrossRef]
7. Koenig, T.K.; Baidar, S.; Campuzano-Jost, P.; Cuevas, C.A.; Dix, B.; Fernandez, R.P.; Guo, H.; Hall, S.R.; Kinnison, D.; Nault, B.A.; et al. Quantitative detection of iodine in the stratosphere. *Proc. Natl. Acad. Sci. USA* **2020**, *117*, 1860–1866. [CrossRef] [PubMed]
8. Klobas, J.E.; Hansen, J.; Weisenstein, D.K.; Kennedy, R.P.; Wilmouth, D.M. Sensitivity of iodine-mediated stratospheric ozone loss chemistry to future chemistry-climate scenarios. *Front. Earth Sci.* **2021**, *9*, 617586. [CrossRef]
9. Klobas, J.E.; Wilmouth, D.M.; Weisenstein, D.K.; Anderson, J.G.; Salawitch, R.J. Ozone depletion following future volcanic eruptions. *Geophys. Res. Lett.* **2017**, *44*, 7490–7499. [CrossRef]
10. Carn, S.A.; Clarisse, L.; Prata, A.J. Multi-decadal satellite measurements of global volcanic degassing. *J. Volcanol. Geotherm. Res.* **2016**, *311*, 99–134. [CrossRef]
11. Theys, N.; Roozendael, M.V.; Dils, B.; Hendrick, F.; Hao, N.; Maziere, M.D. First satellite detection of volcanic bromine monoxide emission after the Kasatochi eruption. *Geophys. Res. Lett.* **2009**, *36*, L03809. [CrossRef]
12. Schönhardt, A.; Richter, A.; Theys, N.; Burrows, J.P. Space-based observation of volcanic iodine monoxide. *Atmos. Chem. Phys.* **2017**, *17*, 4857–4870. [CrossRef]
13. Burkholder, J.B.; Sander, S.P.; Abbatt, J.; Barker, J.R.; Cappa, C.; Crounse, J.D.; Dibble, T.S.; Huie, R.E.; Kolb, C.E.; Kurylo, M.J.; et al. *Chemical Kinetics and Photochemical Data for Use in Atmospheric Studies, Evaluation No. 19*; JPL Publication 19-5; Jet Propulsion Laboratory: Pasadena, CA, USA, 2019. Available online: http://jpldataeval.jpl.nasa.gov (accessed on 30 April 2021).
14. Beach, S.D.; Smith, I.W.M.; Tuckett, R.P. Rate constants for the reaction of Cl atoms with O_3 at temperatures from 298 to 184 K. *Int. J. Chem. Kinet.* **2002**, *34*, 104–109. [CrossRef]
15. Burkholder, J.B.; Hammer, P.D.; Howard, C.J.; Goldman, A. Infrared line intensity measurements in the ν = 0–1 band of the ClO radical. *J. Geophys. Res.* **1989**, *94*, 2225–2234. [CrossRef]
16. Choo, K.Y.; Leu, M.T. Determination of $O_2(^1\Sigma_g{}^+)$ and $O_2(^1\Delta_g)$ yields in Cl + O_2 and Cl + O_3 reactions. *J. Phys. Chem.* **1985**, *89*, 4832–4837. [CrossRef]
17. Clyne, M.A.A.; Nip, W.S. Study of elementary reactions by atomic resonance absorption with a non-reversed source Part 1. The reaction Cl + O_3 → ClO + O_2. *J. Chem. Soc. Faraday Trans. 2* **1976**, *72*, 838–847. [CrossRef]

18. Clyne, M.A.A.; Watson, R.T. Kinetic studies of diatomic free radicals using mass spectrometry Part 2. Rapid bimolecular reactions involving the ClO $X^2\Pi$ radical. *J. Chem. Soc. Faraday Trans.* **1974**, *70*, 2250–2259. [CrossRef]
19. DeMore, W.B. *182nd National Meeting of the American Chemical Society*; American Chemical Society: New York, NY, USA, 1981.
20. DeMore, W.B. Tests of stratospheric models: The reactions of atomic chlorine with O_3 and CH_4 at low temperature. *J. Geophys. Res.* **1991**, *96*, 4995–5000. [CrossRef]
21. Kurylo, M.J.; Braun, W. Flash photolysis resonance fluorescence study of the reaction Cl + O_3 → ClO + O_2 over the temperature range 213–298 K. *Chem. Phys. Lett.* **1976**, *37*, 232–235. [CrossRef]
22. Leu, M.-T.; DeMore, W.B. Rate constants at 295 K for the reactions of atomic chlorine with H_2O_2, HO_2, O_3, CH_4 and HNO_3. *Chem. Phys. Lett.* **1976**, *41*, 121–124. [CrossRef]
23. Nicovich, J.M.; Kreutter, K.D.; Wine, P.H. Kinetics of the reactions of Cl(^2P_J) and Br($^2P_{3/2}$) with O_3. *Int. J. Chem. Kinet.* **1990**, *22*, 399–414. [CrossRef]
24. Seeley, J.V.; Jayne, J.T.; Molina, M.J. Kinetic studies of chlorine atom reactions using the turbulent flow tube technique. *J. Phys. Chem.* **1996**, *100*, 4019–4025. [CrossRef]
25. Vanderzanden, J.W.; Birks, J.W. Formation of oxygen atoms in the reaction of chlorine atoms with ozone. *Chem. Phys. Lett.* **1982**, *88*, 109–114. [CrossRef]
26. Watson, R.T.; Machado, G.; Fischer, S.; Davis, D.D. A temperature dependence kinetics study of the reactions of Cl($^2P_{3/2}$) with O_3, CH_4, and H_2O_2. *J. Chem. Phys.* **1976**, *65*, 2126–2138. [CrossRef]
27. Zahniser, M.S.; Kaufman, F.; Anderson, J.G. Kinetics of the reaction Cl + O_3 → ClO + O_2. *Chem. Phys. Lett.* **1976**, *37*, 226–231. [CrossRef]
28. Clyne, M.A.A.; Watson, R.T. Kinetic studies for diatomic free radicals using mass spectrometry Part 3.-Elementary reactions involving BrO $X^2\Pi$ radicals. *J. Chem. Soc. Faraday Trans.* **1975**, *71*, 336–350. [CrossRef]
29. Leu, M.-T.; DeMore, W.B. Rate constant for the reaction of atomic bromine with ozone. *Chem. Phys. Lett.* **1977**, *48*, 317–320. [CrossRef]
30. Michael, J.V.; Lee, J.H.; Payne, W.A.; Stief, L.J. Absolute rate of the reaction of N(^4S) with NO from 196–400 K with DF-RF and FP-RF techniques. *J. Chem. Phys.* **1978**, *68*, 4093–4097. [CrossRef]
31. Michael, J.V.; Payne, W.A. Absolute rate constants for the reaction of bromine atoms with ozone from 234 to 360 K. *Int. J. Chem. Kinet.* **1979**, *11*, 799–809. [CrossRef]
32. Ninomiya, Y.; Hashimoto, S.; Kawasaki, M.; Wallington, T.J. Cavity ring-down study of BrO radicals: Kinetics of the Br + O_3 reaction and rate of relaxation of vibrationally excited BrO by collisions with N_2 and O_2. *Int. J. Chem. Kinet.* **2000**, *32*, 125–130. [CrossRef]
33. Toohey, D.W.; Brune, W.H.; Anderson, J.G. Rate constant for the reaction Br + O_3 → BrO + O_2 from 248 to 418 K: Kinetics and mechanism. *Int. J. Chem. Kinet.* **1988**, *20*, 131–144. [CrossRef]
34. Buben, S.N.; Larin, I.K.; Messineva, N.A.; Trofimova, E.M. Study of processes with participation of atomic iodine: Determination of a constant of atomic iodine reaction rate with ozone in 231–337 K temperature range. *Khim. Fiz.* **1990**, *9*, 116–126.
35. Tucceri, M.E.; Dillon, T.J.; Crowley, J.N. A laser photolysis-resonance fluorescence study of the reactions: I + O_3 → IO + O_2, O + I_2 → IO + I, and I + NO_2 + M → INO_2 + M at 298 K. *Phys. Chem. Chem. Phys.* **2005**, *7*, 1657–1663. [CrossRef] [PubMed]
36. Sander, S.P. Kinetics and mechanism of the IO + IO reaction. *J. Phys. Chem.* **1986**, *90*, 2194–2199. [CrossRef]
37. Turnipseed, A.A.; Gilles, M.K.; Burkholder, J.B.; Ravishankara, A.R. LIF detection of IO and the rate coefficients for I + O_3 and IO + NO reactions. *Chem. Phys. Lett.* **1995**, *242*, 427–434. [CrossRef]
38. Farantos, S.C.; Murrell, J.N. Classical dynamics of the O + ClO→ Cl + O_2 and Cl + O_3→ ClO + O_2 reactions. *Int. J. Quantum Chem.* **1978**, *14*, 659–674. [CrossRef]
39. Hwang, D.Y.; Mebel, A.M. Ab initio study on the reaction mechanism of ozone with the chlorine atom. *J. Chem. Phys.* **1998**, *109*, 10847–10852. [CrossRef]
40. Tyrrell, J.; Kar, T. A study of the mechanism of the reaction between ozone and the chlorine atom using density functional theory. *J. Phys. Chem. A* **2001**, *105*, 4065–4070. [CrossRef]
41. Castillo, J.F.; Aoiz, F.J.; Martinez-Haya, B. Theoretical study of the dynamics of Cl + O_3 reaction I. Ab initio potential energy surface and quasiclassical trajectory results. *Phys. Chem. Chem. Phys.* **2011**, *13*, 8537–8548. [CrossRef]
42. Li, L.C.; Wang, J.; Wang, X.; Tian, A.M.; Wong, N.B. Quantum chemical study of the reaction mechanism of ozone and methane with fluorine and chlorine atoms. *Int. J. Quantum Chem.* **2002**, *87*, 288–292. [CrossRef]
43. Teixeira, O.B.M.; Marques, J.M.C.; Varandas, A.J.C. Dynamics study of ClO + O_2 collisions and their role in the chemistry of stratospheric ozone. *Phys. Chem. Chem. Phys.* **2004**, *6*, 2179–2184. [CrossRef]
44. Alcami, M.; Cooper, I.L. Ab initio calculations on bromine oxide and dioxides and their corresponding anions. *J. Chem. Phys.* **1998**, *108*, 9414–9424. [CrossRef]
45. Bing, D.; Zhao, Y.; Hao, F.; Li, X.; Liu, F.; Zhang, G.; Zhang, P. Ab initio study on the reaction mechanism of ozone with bromine atom. *Int. J. Quantum Chem.* **2007**, *107*, 1085–1091. [CrossRef]
46. A-Hussein, A.; Drea, A.A. Theoretical investigation study of bromine radical reaction with ozone in stratospheric layer. *J. Appl. Chem.* **2012**, *1*, 453–459.
47. Vijayakumar, S.; Rajakumar, B. Experimental and computational kinetic investigations on the chlorine atom initiated photo-oxidization reaction of butenes in troposphere. *J. Phys. Chem. A* **2017**, *121*, 5487–5499. [CrossRef] [PubMed]

48. Vijayakumar, S.; Kumar, A.; Rajakumar, B. Kinetics of the gas phase reaction of unsaturated ketones with chlorine atoms: An experimental and theoretical investigation. *New J. Chem.* **2017**, *41*, 14299–14314. [CrossRef]
49. Misra, A.; Marshall, P. Computational investigations of iodine oxides. *J. Phys. Chem. A* **1998**, *102*, 9056–9060. [CrossRef]
50. Galvez, O.; Martin, J.C.G.; Gomez, P.C.; Saiz-Lopez, A.; Pacios, L.F. A theoretical study on the formation of iodine oxide aggregates and monohydrates. *Phys. Chem. Chem. Phys.* **2013**, *15*, 15572–15583. [CrossRef]
51. Atkinson, R.; Baulch, D.L.; Cox, R.A.; Crowley, J.N.; Hampson, R.F.; Hynes, R.G.; Jenkin, M.E.; Rossi, M.J.; Troe, J. Evaluated kinetic and photochemical data for atmospheric chemistry: Volume III gas phase reactions of inorganic halogens. *Atmos. Chem. Phys.* **2007**, *7*, 981–1191. Available online: http://www.iupackinetic.ch.cam.ac.uk/ (accessed on 30 April 2021). [CrossRef]
52. Becke, A.D. A multicenter numerical integration scheme for polyatomic molecules. *J. Chem. Phys.* **1988**, *88*, 2547–2553. [CrossRef]
53. Hay, P.J.; Wadt, W.R. Ab initio effective core potentials for molecular calculations. Potentials for the transition metal atoms Sc to Hg. *J. Chem. Phys.* **1985**, *82*, 270–283. [CrossRef]
54. Hill, J.G. Gaussian Basis sets for Molecular Applications. *Int. J. Quantum Chem.* **2013**, *113*, 21–34. [CrossRef]
55. Feller, D.; Peterson, K.A.; Hill, J.G. On the effectiveness of CCSD(T) complete basis set extrapolations for atomization energies. *J. Chem. Phys.* **2011**, *135*, 44102. [CrossRef] [PubMed]
56. Frisch, M.J.; Trucks, G.W.; Schlegel, H.B.; Scuseria, G.E.; Robb, M.A.; Cheeseman, J.R.; Scalmani, G.; Barone, V.; Mennucci, B.; Petersson, G.A.; et al. *Gaussian 09, Revision B.01*; Gaussian, Inc.: Wallingford, CT, USA, 2010.
57. Dennington, I.I.R.; Keith, T.; Millam, J.; Eppinnett, K.; Hovelland, W.L.; Gilliland, R. *GaussView, Version 3.09*; Semichem, Inc.: Shawnee Mission, KS, USA, 2003.
58. Krupicka, M.; Sivalingam, K.; Huntington, L.; Auer, A.A.; Neese, F. A toolchain for the automatic generation of computer codes for correlated wavefunction calculations. *J. Comput. Chem.* **2017**, *38*, 1–16. [CrossRef]
59. Neese, F.; Wennmohs, F.; Becker, U.; Riplinger, C. The ORCA quantum chemistry program package. *J. Chem. Phys.* **2020**, *152*, 224108. [CrossRef] [PubMed]
60. Shepard, R.; Shavitt, I.; Pitzer, R.M.; Comeau, D.C.; Pepper, M.; Lischka, H.; Szalay, P.G.; Ahlrichs, R.; Brown, F.B.; Zhao, J. A progress report on the status of the COLUMBUS MRCI program system. *Int. J. Quantum Chem. Quantum Chem. Symp.* **1988**, *22*, 149–165. [CrossRef]
61. Buenker, R.J.; Peyerimhoff, S.D. Individualized configuration selection in CI calculations with subsequent energy extrapolation. *Theoret. Chim. Acta* **1974**, *35*, 33–58. [CrossRef]
62. Gonzalez-Lafont, A.; Truong, T.N.; Truhlar, D.G. Interpolated variational transition state theory: Practical methods for estimating variational transition state properties and tunneling contributions to chemical reaction rates from electronic structure calculations. *J. Chem. Phys.* **1991**, *95*, 8875–8894. [CrossRef]
63. Lu, D.H.; Truong, T.N.; Melissas, V.S.; Lynch, G.C.; Liu, Y.P.; Garrett, B.C.; Steckler, R.; Isaacson, A.D.; Rai, S.N.; Hancock, G.C.; et al. POLYRATE 4. *Comput. Phys. Commun.* **1992**, *71*, 235–262. [CrossRef]
64. Karmakar, S.; Datta, A. Tunneling assists the 1,2-Hydrogen shift in N-Heterocyclic carbenes. *Angew. Chem. Int. Ed.* **2014**, *53*, 9587–9591. [CrossRef] [PubMed]
65. Vijayakumar, S.; Wilmouth, D.M. Atmospheric fate of formyl chloride and mechanisms of the gas-phase reactions with OH radicals and Cl atoms. *Chem. Phys. Lett.* **2021**, *777*, 138709. [CrossRef]
66. Molina, M.J.; Rowland, F.S. Stratospheric sink for chlorofluoromethanes: Chlorine atom-catalysed destruction of ozone. *Nature* **1974**, *249*, 810–812. [CrossRef]
67. Dyke, J.M.; Gamblin, S.D.; Hooper, N.; Lee, E.P.F.; Morris, A.; Mok, D.K.W.; Chau, F.T. A study of the BrO and BrO_2 radicals with vacuum ultraviolet photoelectron spectroscopy. *J. Chem. Phys.* **2000**, *112*, 6262–6274. [CrossRef]